

# Surface Plasmon Polaritons Based Non-All-Optical Four-Wave Mixing

Qun Zhang,<sup>1\*</sup> Ke Lin,<sup>1</sup> and Yi Luo<sup>1,2\*</sup>

<sup>1</sup>*Hefei National Laboratory of Physical Sciences at the Microscale and Department of Chemical Physics,  
University of Science and Technology of China, Hefei, Anhui 230026, P. R. China*

<sup>2</sup>*Department of Theoretical Chemistry, School of Biotechnology,  
Royal Institute of Technology, AlbaNova, S-106 91 Stockholm, Sweden*

\*Authors to whom correspondence should be addressed: [qunzh@ustc.edu.cn](mailto:qunzh@ustc.edu.cn) & [yiluo@ustc.edu.cn](mailto:yiluo@ustc.edu.cn).

**Abstract.**—A novel concept of non-all-optical four-wave mixing (NAO-4WM) is put forward, in which a laser-launched evanescent field of surface plasmon polaritons (SPPs) is utilized as a coherent non-optical pumping source to involve directly in a nonlinear 4WM process at the dielectric/metal interface. Conversion efficiency of the resultant 4WM radiation is expected to be dramatically increased due to the local-field enhancement effect induced by SPPs. Feasibility of implementing this concept at the air/gold and graphene/gold interfaces is further examined by numerical simulations. The concept developed here together with its effective integration with graphene shows intriguing promise for newly emerging applications in nano-photonics, optoelectronics, and active plasmonics.

**PACS numbers:** 73.20.Mf, 78.68.+m, 42.65.Hw, 78.67.Wj

**Introduction.**—Surface plasmon polaritons (SPPs) are guided electromagnetic waves that propagate along the interface of a metal and a dielectric material as a result of collective electron oscillations coupled to an external optical field [1]. Triggered by rapid advances in nanofabrication and near-field optical microscopy, intensified SPPs-related research activities emerged in recent years [2-5]. Noticeably, the coherent nature of the evanescent SPP surface wave [6] has recently been “visualized” in a straightforward fashion in an elegant “double-slit” experiment with SPPs [7]. It would thus be expected that SPPs may, in principle, be able to participate directly (and coherently) in conventional nonlinear optical processes of fundamental and practical interest, such as sum-frequency generation and four-wave mixing [8].

We propose here a new concept of SPPs-based non-all-optical four-wave mixing (NAO-4WM), the essence of which lies in that an evanescent SPP field localized at a dielectric/metal interface, though *nonradiative* (yet *coherent*), can be employed to interact *directly* with an additional propagating optical field, giving rise to a nonlinear surface 4WM field in a coherent manner. We show that the conversion efficiency of the resultant 4WM radiation can be significantly increased due to the SPPs-induced local-field enhancement effect. We examine the concept by performing numerical simulations for two types of SPPs-based NAO-4WM at the air/gold interface. Furthermore, an extension to the graphene/gold interface is presented. Our simulated two-dimensional wavelength-dependent angular distributions (2D-WAD) spectra provide straightforward guiding maps for further experimental verification.

It should be pointed out that the realization of nonlinear 4WM on metal surfaces is not totally new in itself. Very recently, Novotny and co-workers [9] have demonstrated that nonlinear excitation of SPPs can be directly accomplished on a gold film by optical 4WM, and further, both

propagating and evanescent 4WM waves can be generated by vectorially adding the in-plane momenta of incident photons at the air/gold interface. In contrast to these pioneering contributions that are basically in the *all-optical* domain (in terms of the optical pumping sources that directly participate in 4WM), the new concept developed here distinguishes itself in that an evanescent in-plane SPP wave, at the very moment of being established at a dielectric/metal interface, is employed to take the place of one of the optical pumping fields used for converting into a 4WM field; in other words, ensured by its coherent nature [6,7], the non-optical SPP field (albeit excited optically) acts as a *direct pumping source* in surface 4WM.

In the context of nonlinear 4WM, the proposed concept should be well-grounded in logic, for no evidence seems to bolster such an assertion that a certain one of the four (pumping or emitted) fields involved in 4WM may enjoy a sort of “privilege” over the others. To put it in another way, now that the emitted 4WM field can be purely evanescent (nonradiative) as confirmed by Ref. [9], so can be any one of the 4WM pumping fields. It is therefore conceivable that the SPPs-based NAO-4WM processes should be able to effectively take place at the dielectric/metal interface, provided that all the involved fields are coherent, *irrespective of being optical or non-optical*. Most importantly, one would expect to take full advantage of the significant local-field enhancement effect [10] induced by SPPs to considerably enhance its conversion efficiency, a feat that would otherwise be unattainable in conventional all-optical 4WM processes.

**Local-field enhancement.**—We consider here an SPPs-based NAO-4WM process [11] at the air/gold interface. Of particular interest are the two schemes [(a) and (b)] depicted in the top panels of Fig. 1:

$$\omega_{4wm(a)} = 2\omega_{spp} - \omega_{opt} \quad [\text{Scheme (a)}], \quad (1)$$

and  $\omega_{4\text{wm(b)}} = 2\omega_{\text{opt}} - \omega_{\text{spp}}$  [Scheme (b)]. (2)

Here, the SPP field with frequency  $\omega_{\text{spp}}$  is launched by an external optical field ( $\lambda_{\text{exc}}$ ) in the Kretschmann-Raether (KR) geometry [12]. A second optical field at  $\omega_{\text{opt}}$  is introduced to interact with the SPP field at the air/gold interface, giving rise to the coherent 4WM radiative fields with frequencies  $\omega_{4\text{wm(a)}}$  or  $\omega_{4\text{wm(b)}}$ . The third-order susceptibility of gold,  $\chi_{\text{Au}}^{(3)}$ , induces nonlinear surface polarizations for both schemes:

$$P^{(\text{a})}(\omega_{4\text{wm(a)}} = 2\omega_{\text{spp}} - \omega_{\text{opt}}) = \epsilon_0 \chi_{\text{Au}}^{(3)}(-\omega_{4\text{wm(a)}}; \omega_{\text{spp}}, \omega_{\text{spp}}, -\omega_{\text{opt}}) E_{\text{spp}}(\omega_{\text{spp}}) E_{\text{spp}}(\omega_{\text{spp}}) E_{\text{opt}}^*(\omega_{\text{opt}}), \quad (3)$$

and  $P^{(\text{b})}(\omega_{4\text{wm(b)}} = 2\omega_{\text{opt}} - \omega_{\text{spp}}) = \epsilon_0 \chi_{\text{Au}}^{(3)}(-\omega_{4\text{wm(b)}}; \omega_{\text{opt}}, \omega_{\text{opt}}, -\omega_{\text{spp}}) E_{\text{opt}}(\omega_{\text{opt}}) E_{\text{opt}}(\omega_{\text{opt}}) E_{\text{spp}}^*(\omega_{\text{spp}}), \quad (4)$

where  $E_{\text{spp}}(\omega_{\text{spp}})$  and  $E_{\text{opt}}(\omega_{\text{opt}})$  are the electric fields associated with the in-plane SPP wave and the propagating  $\omega_{\text{opt}}$  beam, respectively, and  $\epsilon_0$  is the permittivity of free space.

Still with Scheme (a), if the non-optical SPP field is replaced with the propagating optical field ( $\lambda_{\text{exc}}$ ) that is originally used to excite the SPP wave, the corresponding all-optical 4WM process [denoted as (a')] [9] may, alternatively, be expressed by a nonlinear polarization according to

$$P^{(\text{a}')}(2\omega_{\text{exc}} - \omega_{\text{opt}}) = \epsilon_0 \chi_{\text{Au}}^{(3)}(-\omega_{4\text{wm(a')}}; \omega_{\text{exc}}, \omega_{\text{exc}}, -\omega_{\text{opt}}) E_{\text{exc}}(\omega_{\text{exc}}) E_{\text{exc}}(\omega_{\text{exc}}) E_{\text{opt}}^*(\omega_{\text{opt}}), \quad (5)$$

where  $E_{\text{exc}}(\omega_{\text{exc}})$  is the electric field associated with the SPP-excitation light ( $\lambda_{\text{exc}}$ ) that carries exactly the same frequency as the SPP wave does, a consequence of energy conservation, i.e.,  $\omega_{\text{exc}} (= 2\pi c / \lambda_{\text{exc}}) \equiv \omega_{\text{spp}}$ . Obviously, Eq. (5) differs from Eq. (3) only in  $E_{\text{exc}}(\omega_{\text{exc}})$ , and thereby the SPPs-induced local-field intensity enhancement,  $G$ , under this particular scheme reads

$$G = \left| \frac{E_{\text{spp}}(\omega_{\text{spp}})}{E_{\text{exc}}(\omega_{\text{spp}})} \right|^4, \quad (6)$$

an expression quite similar to  ${}^{\text{em}}G_{\text{SERS}}$  (as large as  $10^5 - 10^6$ ) that is, to a first approximation, responsible for the electromagnetic enhancement of Raman signals in surface-enhanced Raman scattering (SERS) [13]. Alternatively, if switching from Scheme (a) to Scheme (b) one would still

expect a quite high enhancement (to the second power of  $|E_{\text{spp}}(\omega_{\text{spp}})/E_{\text{exc}}(\omega_{\text{spp}})|$ ). It is generally agreed that the physics underlying such high enhancements stems from the excitation of electromagnetic resonances in the metallic structures that permits a highly concentrated field at the very surface of metal film [2,3].

**2D-WAD spectra: Scheme (a).**—Irrespective of being all-optical or non-all-optical, 4WM must obey both energy and momentum conservations. Equations (1) and (2) are statements of energy conservation, defining the frequencies of the outgoing 4WM radiation. To effectively generate the emitted 4WM radiation, one must also ensure phase-matching of the four fields involved in 4WM.

Let us first interrogate Scheme (a). Depending on the incidence directions of the  $\omega_{\text{opt}}$  beam two possible configurations may be considered, as sketched in panels (a1) and (a2) of Fig. 1. Propagation of the  $\omega_{\text{opt}}$  beam is kept in-plane with that of the SPP-excitation beam ( $\lambda_{\text{exc}}$ ), and both beams are *p*-polarized. Without losing generality, the  $\lambda_{\text{exc}}$  beam is confined in the third quadrant of x-z plane perpendicular to the metal surface, making the SPP wave vector pointing to the +x direction. All the angles are measured from the surface normal in clockwise direction. To excite SPPs at the air/gold interface, we here use a modified KR configuration that consists of a hemisphere glass prism and a thin film of gold (thickness typically below 100 nm) deposited on the planar surface of the substrate.

As for the first configuration [Fig. 1(a1)] where the  $\omega_{\text{opt}}$  beam impinges on the metal surface from the air side, momentum conservation defines the propagation directions according to

$$k_{4\text{wm}(a)} \sin \theta_{4\text{wm}(a)} = 2 \operatorname{Re}(k_{\text{spp}}) + k_{\text{opt}} \sin \theta_{\text{opt}}, \quad (7)$$

$$k_{4\text{wm}(a)} \cos \theta_{4\text{wm}(a)} = k_{\text{opt}} \cos \theta_{\text{opt}}, \quad (8)$$

$$\text{where } k_{4\text{wm(a)}} = \omega_{4\text{wm(a)}} / c, \quad k_{\text{opt}} = \omega_{\text{opt}} / c, \text{ and } k_{\text{spp}} = \frac{\omega_{\text{spp}}}{c} \sqrt{\frac{\epsilon_d \epsilon_m(\omega_{\text{spp}})}{\epsilon_d + \epsilon_m(\omega_{\text{spp}})}} \quad [2], \quad (9)$$

$\epsilon_m(\omega_{\text{spp}})$  is the frequency-dependent complex dielectric function of the metal (data for gold taken from Ref. [14]) and  $\epsilon_d$  is the dielectric constant of the superstrate material ( $\epsilon_d = 1$  for air).

Equations (7)–(9) combined with Eq. (1) yield the two sets of angle of interest:

$$\theta_{\text{opt}} = \arcsin\left(\frac{1-\eta^2}{\eta} \frac{\lambda_{\text{opt}}}{\lambda_{\text{exc}}} - \frac{1}{\eta}\right), \quad (10)$$

$$\theta_{4\text{wm(a)}} = \arcsin\left(\frac{1+\eta^2}{\eta} \frac{\lambda_{4\text{wm(a)}}}{\lambda_{\text{exc}}} - \frac{1}{\eta} \frac{\lambda_{4\text{wm(a)}}}{\lambda_{\text{opt}}}\right), \quad (11)$$

$$\text{where } \lambda_{\text{exc}} = 2\pi c / \omega_{\text{spp}}, \quad \lambda_{\text{opt}} = 2\pi c / \omega_{\text{opt}}, \quad \lambda_{4\text{wm(a)}} = 2\pi c / \omega_{4\text{wm(a)}}, \quad (12)$$

$$\text{and } \eta = \text{Re}\left(\sqrt{\frac{\epsilon_d \epsilon_m(\omega_{\text{spp}})}{\epsilon_d + \epsilon_m(\omega_{\text{spp}})}}\right). \quad (13)$$

Note that  $\eta [= \eta(\lambda_{\text{exc}}) = \eta(\omega_{\text{spp}})]$  is usually referred to as the effective refractive index [15], the real part of the ratio of  $k_{\text{spp}}$  to the free-space wave vector [ $2\pi/\lambda_{\text{exc}} (= \omega_{\text{spp}}/c)$ ]. The wavelength-dependent SPP-excitation angle,  $\theta_{\text{spp}}(\lambda_{\text{exc}})$ , is simply determined by

$$\sin \theta_{\text{spp}}(\lambda_{\text{exc}}) = \eta(\lambda_{\text{exc}}) / n_s, \quad (14)$$

where  $n_s$  is the refractive index of the substrate ( $n_s \approx 1.5$  for BK7 glass used here). This specific incidence angle allows matching of the SPP wave vector by the light wave-vector component parallel to the surface, thereby generating the evanescent SPP wave at the metal surface [1,2].

When both  $\lambda_{\text{exc}}$  and  $\lambda_{\text{opt}}$  are scanned from 350 to 1200 nm in a 1 nm step, Eqs. (10) and (11) yield the simulated 2D-WAD spectra of  $\theta_{\text{opt}}(\lambda_{\text{exc}}, \lambda_{\text{opt}})$  [Fig. 2(a)] and  $\theta_{4\text{wm(a)}}(\lambda_{\text{exc}}, \lambda_{\text{opt}})$  [Fig. 2(b)]. It is seen that the momentum conservation restricts  $\lambda_{\text{exc}}$  to below 417 nm (while  $\lambda_{\text{opt}}$  could be anywhere in 350–1200 nm), and hence  $\lambda_{4\text{wm(a)}}$  to within a range of 205–515 nm [Fig. 2(c)]. Interestingly, in this particular configuration the propagation of the  $\lambda_{\text{opt}}$  beam must be confined

to the second quadrant ( $\theta_{\text{opt}} < 0$ ) and is nearly parallel to the surface (close to the so-called “grazing incidence”), while the outgoing 4WM radiation is expected to be detectable only in the first quadrant ( $\theta_{4\text{wm(a)}} > 0$ ) and also nearly parallel to the surface ( $\theta_{4\text{wm(a)}} \in [84.3^\circ, 89.5^\circ]$ ). Admittedly, such an observation together with the very narrow ( $< 6^\circ$ ) range available for  $\theta_{4\text{wm(a)}}$  may affiliate, to a certain extent, the proof-of-principle experiments using this configuration. However, this can be easily overcome by means of narrow bandpass filtering combined with routinely available high-sensitivity detection techniques (e.g., photon counting).

We turn now to the second configuration of Scheme (a), as depicted in Fig. 1(a2). Unlike the first one, this configuration features an  $\omega_{\text{opt}}$  beam incident from the glass (instead of air) side. A simple vectorial algebra reveals immediately that the outgoing 4WM beam (if existing) has to radiate also in the lower half-space. The fact that both beams propagate in the lower half-space suggests that (i)  $n_s$  must be taken into account, (ii)  $\lambda_{4\text{wm(a)}} < 350 \text{ nm}$  due to the transmission property of BK7 glass, and (iii) those nominal solutions of  $(\lambda_{\text{exc}}, \lambda_{\text{opt}})$  with corresponding  $\theta_{\text{opt}}$  equivalent to or larger than the total internal reflection angle should be invalidated. In spite of these constraints, the obtained spectra [Figs. 2(d)-2(f)] turn out to permit a much better angle and wavelength tunability:  $\theta_{\text{opt}} \in [-5.2^\circ, 41.8^\circ]$ ,  $\theta_{4\text{wm(a)}} \in [-73.1^\circ, -41.4^\circ]$ , and  $\lambda_{4\text{wm(a)}} \in [350 \text{ nm}, 1182 \text{ nm}]$ .

**2D-WAD spectra: Scheme (b).**— Although Scheme (b) is less competitive than Scheme (a) in terms of the ability to increase the SPPs-based NAO-4WM efficiency, it is still capable of bringing forth an enhancement that is pronounced when compared to its all-optical counterpart. Therefore, it is necessary to gain insight into its feasibility. This scheme may also be arranged in two configurations, as sketched in Figs. 1(b1) and 1(b2). Simulations indicate that although the configuration shown in Fig. 1(b2) does not work, the one shown in Fig. 1(b1) not only works but

offers a best tunability:  $\theta_{\text{opt}} \in [-81.2^\circ, 40.6^\circ]$ ,  $\theta_{4\text{wm(b)}} \in [-38.9^\circ, 49.2^\circ]$ , and  $\lambda_{4\text{wm(b)}} \in [350 \text{ nm}, 2000 \text{ nm}]$  [Figs. 2(g)-2(i)].

Interestingly, among the four configurations of the two schemes discussed above, the only one that fails to generate the NAO-4WM radiation belongs to Scheme (b). As for the preferred Scheme (a), from an experimental point of view, it would be highly recommended to adopt the second configuration in light of the better accessibility and tunability for both wavelength and angle it offers.

*An extension to the graphene/gold interface.*—The conceptual experiments presented in this Letter are associated with, but not limited to, the air/gold interface. Our choice of gold here is mainly based on its several merits: (i)  $\chi_{\text{Au}}^{(3)}$  is quite large [16,17], (ii) its chemical stability is high and its handling is convenient [3], and (iii) the resonant SPP-excitation on a gold film is usually in the desirable visible (or near infrared) spectral region [2]. When air ( $\varepsilon_{\text{air}} = 1$ ) is replaced with other dielectric materials ( $\varepsilon_d$ ), the concept may also be feasible given that SPPs can be launched and sustained by such dielectric/metal surfaces.

We present here an extended case study of SPPs-based NAO-4WM at the interface of graphene [18] and gold. The effective  $\chi_{\text{Gr}}^{(3)}$  of graphene [19] has been determined to be  $\sim 8$  orders of magnitude and  $\sim 40$ -fold larger than that of glass and the quasi-2D thin film of gold, respectively. We thus envisage that such an exceptionally high nonlinear response of graphene would allow for another 1–2 orders of magnitude enhancement of the third-order nonlinear conversion efficiency, provided that the marriage of our concept and the graphene/gold interface is feasible. More importantly, because interband electron transitions in graphene can occur at all energies as a result of its unique linear band structure [18], such a marriage can be expected to generate both

frequency and angle tunable, significantly enhanced, nonlinear surface 4WM radiation, hence showing enticing potentials for graphene-based nano-photonic and optoelectronic devices.

As in the air/gold case, SPPs-based NAO-4WM at the graphene/gold interface may also be implemented through two schemes [top panel of Fig. 3]. Since the SPP field along the z direction retains within the nanometer scale [2], the graphene sample deposited on the gold film can be single or multi-layered. In our conceptual experiment here, a dielectric with a large  $n_s$  value of 2.2 is chosen for effectively launching SPPs at the graphene/gold interface.  $\lambda_{\text{exc}}$  and  $\lambda_{\text{opt}}$  are scanned in 400–525 nm (where  $n_{\text{Gr}}$  takes a nearly constant value of  $\sim 2.7$  [20]) and 400–1200 nm, respectively. Our simulations indicate that Scheme (a) works solely for the configuration sketched in Fig. 1(a2). The obtained spectra are given in Figs. 3(a)–3(c), from which one can detect that a fairly broad ( $\sim 65$ -nm) tunable range of  $\lambda_{\text{4wm}(a)}$  can be achieved in the UV (256–321 nm) although the angle tunability is limited ( $\theta_{\text{opt}} \in [17^\circ, 27^\circ]$  and  $\theta_{\text{4wm}(a)} \in [-79^\circ, -73.4^\circ]$ ). Here, it should be emphasized that thus obtained NAO-4WM radiation is estimated to be enhanced by 5–6 orders of magnitude (due to the SPPs-induced local-field enhancement effect) when compared to that achieved at the graphene/glass interface [19], and by 1–2 orders of magnitude when compared to that achieved at the air/gold interface (due to  $\chi_{\text{Gr}}^{(3)} / \chi_{\text{Au}}^{(3)} \approx 40$  [17,19]). Moreover, it turns out that Scheme (b) works only for the configuration sketched in Fig. 1(b1) [simulated spectra shown in Figs. 3(d)–3(f)]. Notwithstanding Scheme (b) is less efficient than Scheme (a) in terms of the enhancement  $G$  factor, it not only compensates for the lack of angle tunability ( $\theta_{\text{opt}} \in [-89.9^\circ, 7.5^\circ]$  and  $\theta_{\text{4wm}(b)} \in [30^\circ, 89.8^\circ]$ ) but enables a much better wavelength tunability ( $\lambda_{\text{4wm}(b)} \in [323 \text{ nm}, 1845 \text{ nm}]$ ). The two schemes are complementary to each other in this case.

**Concluding remarks.**—To summarize, we have developed a new concept of non-all-optical

four-wave mixing based on surface plasmon polaritons. Directly involving in the third-order nonlinear process at the dielectric/metal interface, the evanescent SPP field coherently imparts its intrinsic local-field enhancement effect to the resultant surface 4WM radiation, thereby dramatically increasing its conversion efficiency. Conceptual experiments have been performed through numerical simulations for various possible configurations at the air/gold interface with their feasibility carefully examined. We have further exploited the possibilities of incorporating the concept with the unique linear band structure as well as remarkably strong nonlinear optical response of graphene, towards generating significantly enhanced, both frequency and angle tunable, directional, and coherent surface four-wave mixing radiation. We believe that this new concept together with its effective integration with graphene may open opportunities for applications in nano-photonics, optoelectronics, and active plasmonics.

*Acknowledgements.*— This work is supported by the Major State Basic Research Development Programs of China (2010CB923300, 2007CB815203), the National Natural Science Foundation of China (20873133, 20925311), and the Chinese Academy of Sciences (KJCX2- YW-N24).

## References

- [1] H. Raether, *Surface Plasmons* (Springer-Verlag, Berlin, 1988).
- [2] A. V. Zayats, I. I. Smolyaninov, and A. A. Maradudin, Phys. Rep. **408**, 131 (1995), and references therein.
- [3] J. R. Krenn and J.-C. Weeber, Phil. Trans. R. Soc. Lond. A **362**, 739 (2004), and references therein.
- [4] *Surface Plasmon Nanophotonics*, edited by M. L. Brongersma and P. G. Kik (Springer, Dordrecht, 2007).
- [5] S. A. Maier, *Plasmonics: Fundamentals and Applications* (Springer, New York, 2007).
- [6] H. Raether, in *physics of thin films*, edited by G. Hass, M. H. Francombe, and R. W. Hoffman (Academic Press, New York, 1977), Vol. 9, Chap. 3, pp 145-262.
- [7] R. Zia and M. L. Brongersma, Nat. Nanotech. **2**, 426 (2007).
- [8] Y. R. Shen, *The Principles of Nonlinear Optics* (John Wiley & Sons, New York, 1988).
- [9] S. Palomba and L. Novotny, Phys. Rev. Lett. **101**, 056802 (2008); J. Renger *et al.*, Phys. Rev. Lett. **103**, 266802 (2009); J. Renger *et al.*, Phys. Rev. Lett. **104**, 046803 (2010).
- [10] G. T. Boyd, Th. Rasing, J. R. R. Leite, and Y. R. Shen, Phys. Rev. B **30**, 519 (1984), and references therein; S. I. Bozhevolnyi, J. Beermann, and V. Coello, Phys. Rev. Lett. **90**, 197403 (2003).
- [11] The concept developed here for 4WM can be readily extended to other nonlinear optical processes, such as SFG and DFG [8], for which we have also performed simulations indicating that they work as well under certain conditions (not shown here).
- [12] E. Kretschmann and H. Raether, Z. Naturforsch. A **23**, 2135 (1968).
- [13] M. Moskovits, Rev. Mod. Phys. **57**, 783 (1985); F. J. García-Vidal and J. B. Pendry, Phys. Rev. Lett. **77**, 1163 (1996).
- [14] D. W. Lynch and W. R. Hunter, in *Handbook of Optical Constants of Solids*, edited by E. Palik (Academic Press, Orlando, 1985), pp 286-295.
- [15] A. V. Krasavin and A. V. Zayats, Opt. Lett. **35**, 2118 (2010).
- [16] R. A. Ganeev *et al.*, Opt. Commun. **229**, 403 (2004).
- [17] E. Xenogiannopoulou *et al.*, Opt. Commun. **275**, 217 (2007).
- [18] A. K. Geim and K. S. Novoselov, Nat. Mater. **6**, 183 (2007); A. K. Geim, Science **324**, 1530 (2009); A. H. Castro Neto *et al.*, Rev. Mod. Phys. **81**, 109 (2009).
- [19] E. Hendry *et al.*, Phys. Rev. Lett. **105**, 097401 (2010).
- [20] J. W. Weber, V. E. Calado, and M. C. M. van de Sanden, Appl. Phys. Lett. **97**, 091904 (2010).

**FIG. 1.** (by Zhang, Lin, and Luo)

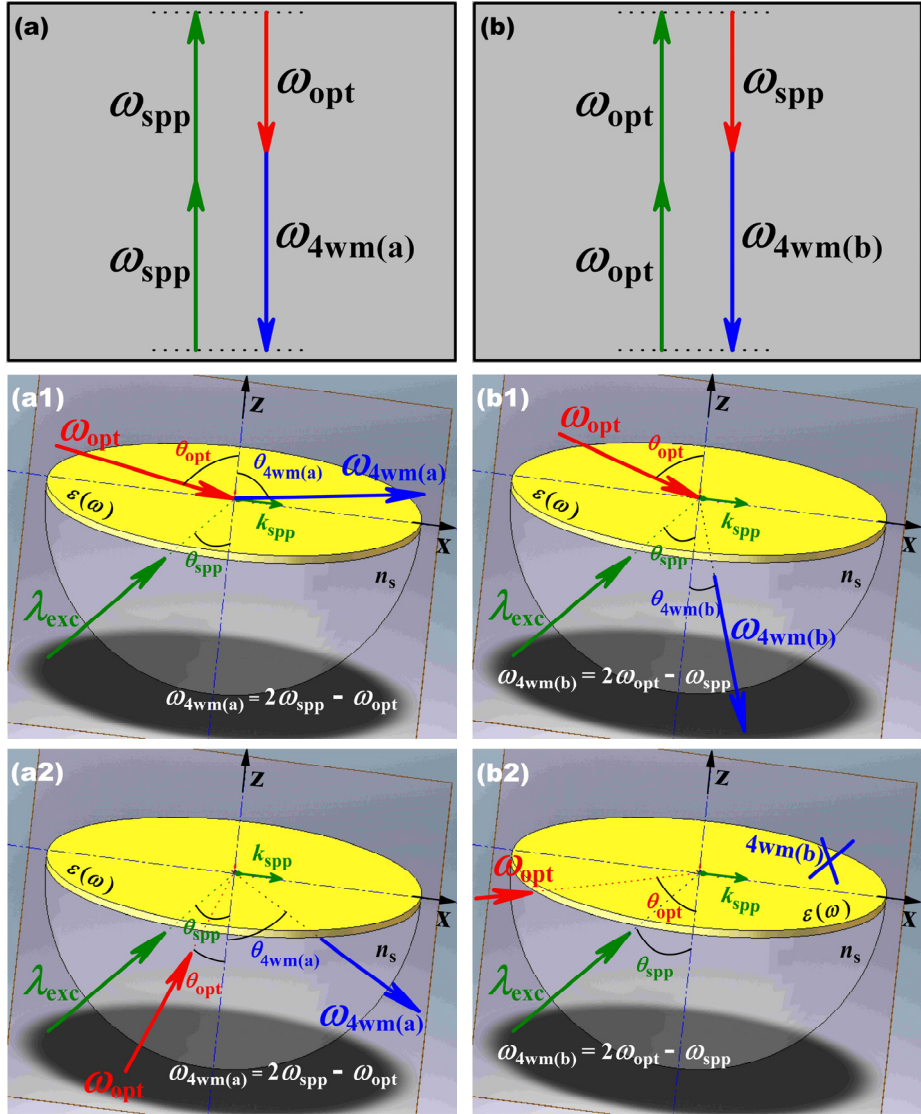


**FIG. 1 (color online).** Diagram of the two SPPs-based NAO-4WM schemes [(a)  $\omega_{4\text{wm(a)}} = 2\omega_{\text{spp}} - \omega_{\text{opt}}$ ; (b)  $\omega_{4\text{wm(b)}} = 2\omega_{\text{opt}} - \omega_{\text{spp}}$ ] and sketches of the corresponding configurations for the case of air/gold interface (see text for details).

**FIG. 2. (by Zhang, Lin, and Luo)**

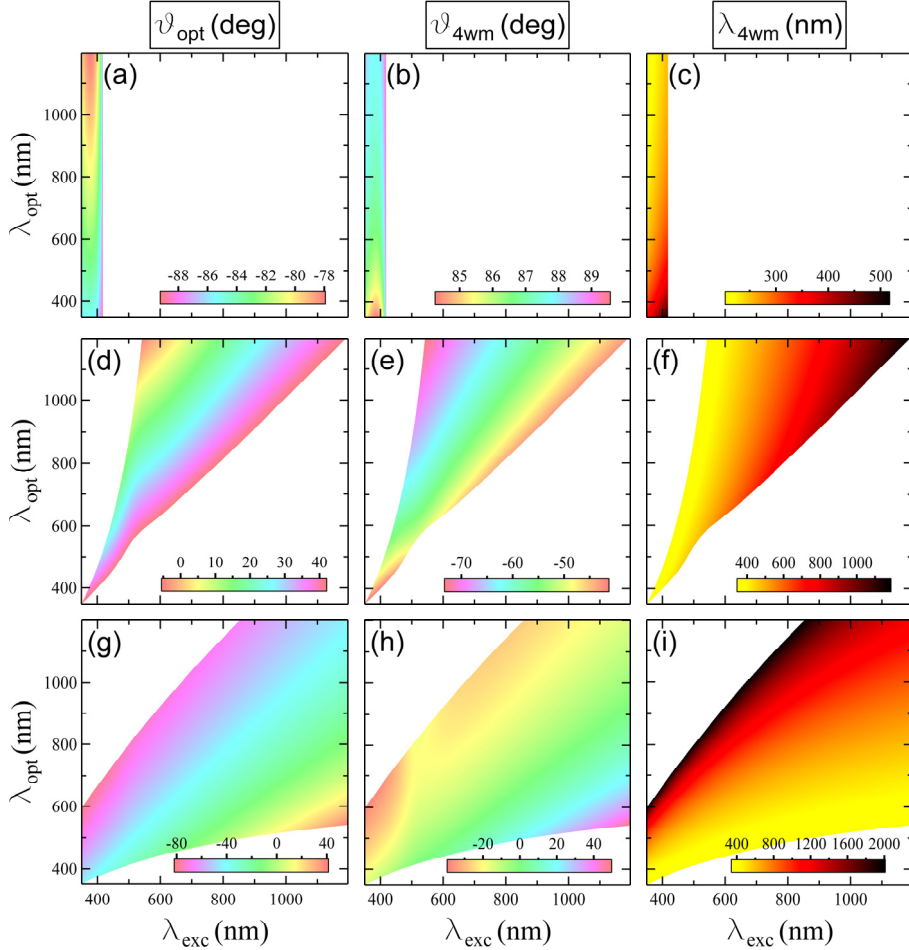


**FIG. 2 (color online).** 2D-WAD spectra of  $\theta_{\text{opt}}(\lambda_{\text{exc}}, \lambda_{\text{opt}})$  (left column) and  $\theta_{\text{4wm}}(\lambda_{\text{exc}}, \lambda_{\text{opt}})$  (middle column), and the corresponding 4WM wavelength distributions (right column) for the case of air/gold interface. The top, middle, and bottom rows correspond, respectively, to the configurations (a1), (a2), and (b1) shown in Fig. 1.

**FIG. 3.** (by Zhang, Lin, and Luo)

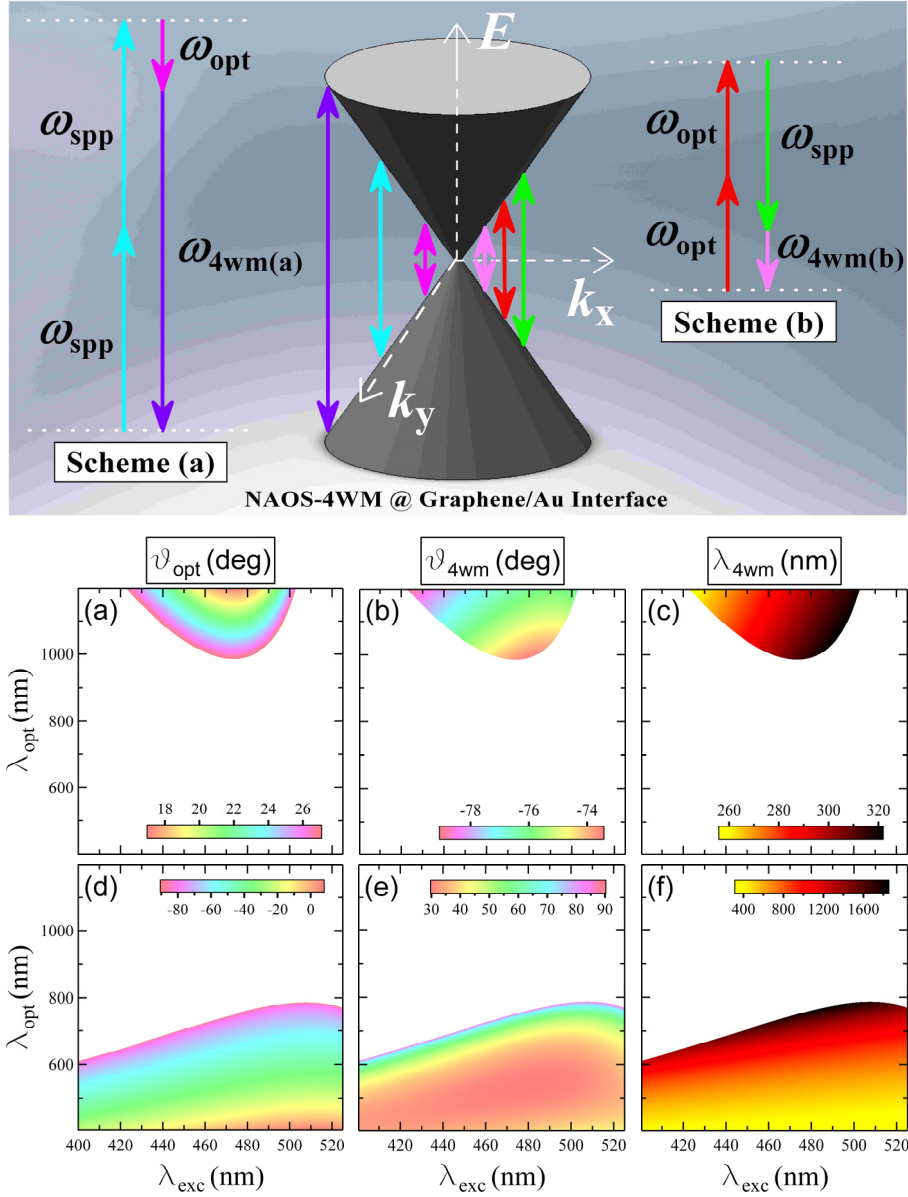


**FIG. 3 (color online).** Schematic of graphene's band structure with three resonant-field energies (double arrows) involved in the two schemes of SPPs-based NAO-4WM. Panels (a)–(f) exhibit the 2D-WAD spectra of  $\theta_{\text{opt}}(\lambda_{\text{exc}}, \lambda_{\text{opt}})$  [(a) and (d)] and  $\theta_{4\text{wm}}(\lambda_{\text{exc}}, \lambda_{\text{opt}})$  [(b) and (e)], and the corresponding 4WM wavelength distributions [(c) and (f)]. Panels (a), (b), and (c) correlate with Scheme (a); panels (d), (e), and (f) correlate with Scheme (b).

**FIG. 2 supplemental.** (by Zhang, Lin, and Luo)

For the case of air/gold interface, we have also performed numerical simulations for the **efficiencies of the three NAO-4WM processes** (whose 2D-WAD spectra and 4WM wavelength distributions are illustrated in Fig. 2, see text). The simulated results (shown below in the middle and right columns) are obtained based on Ref. [9] [J. Renger *et al.*, Phys. Rev. Lett. **104**, 046803 (2010)] and a reasonable assumption of  $|E_{\text{spp}}| = 10 \times |E_{\text{opt}}|$ .

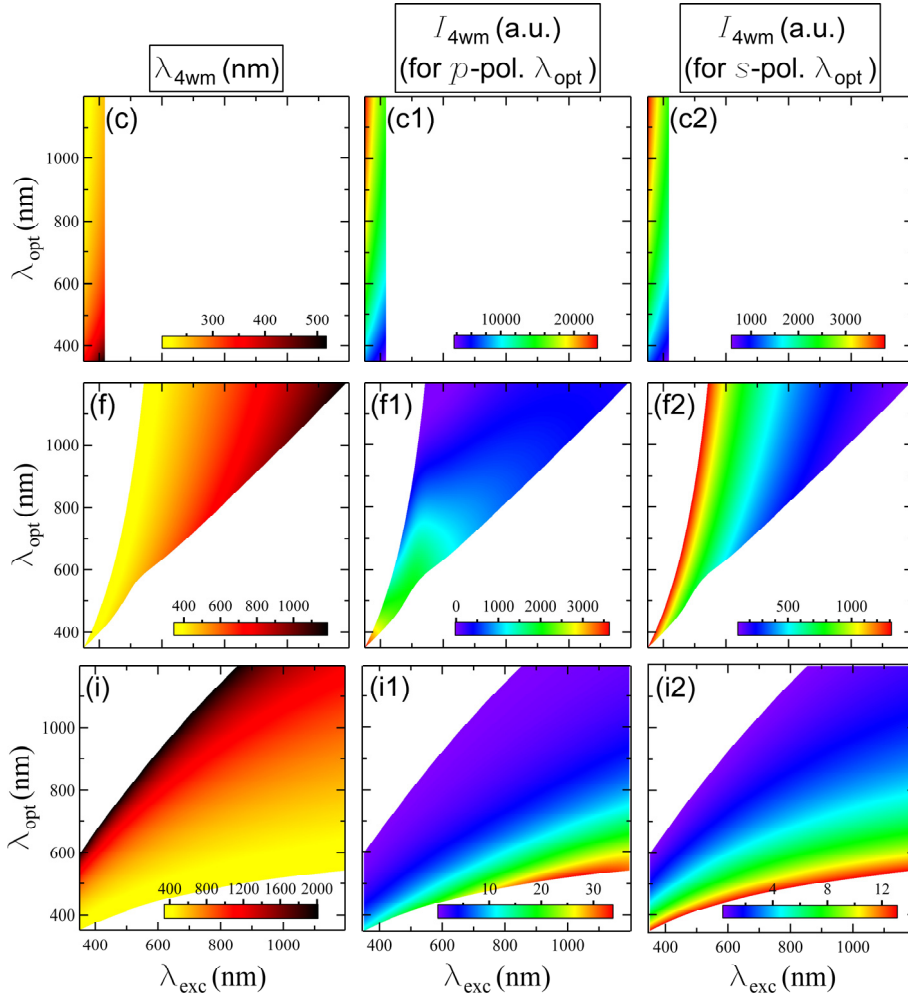


**FIG. 2\_supplemental.** The 4WM wavelength distributions [(c), (f), and (i), see also Fig. 2] and their corresponding efficiencies ( $|E_{\text{4wm}}|^2$ ) for two particular cases: (1) the  $\lambda_{\text{opt}}$  beam is **p-polarized** [(c1), (f1), and (i1)]; (2) the  $\lambda_{\text{opt}}$  beam is **s-polarized** [(c2), (f2), and (i2)]. As in Fig. 2, the top, middle, and bottom rows correspond, respectively, to the configurations (a1), (a2), and (b1) shown in Fig. 1 (see text for details).